Volume 9 | Number 21 | 7 June 2018 | Pages 4721–4920

Chemical Science

rsc.li/chemical-science

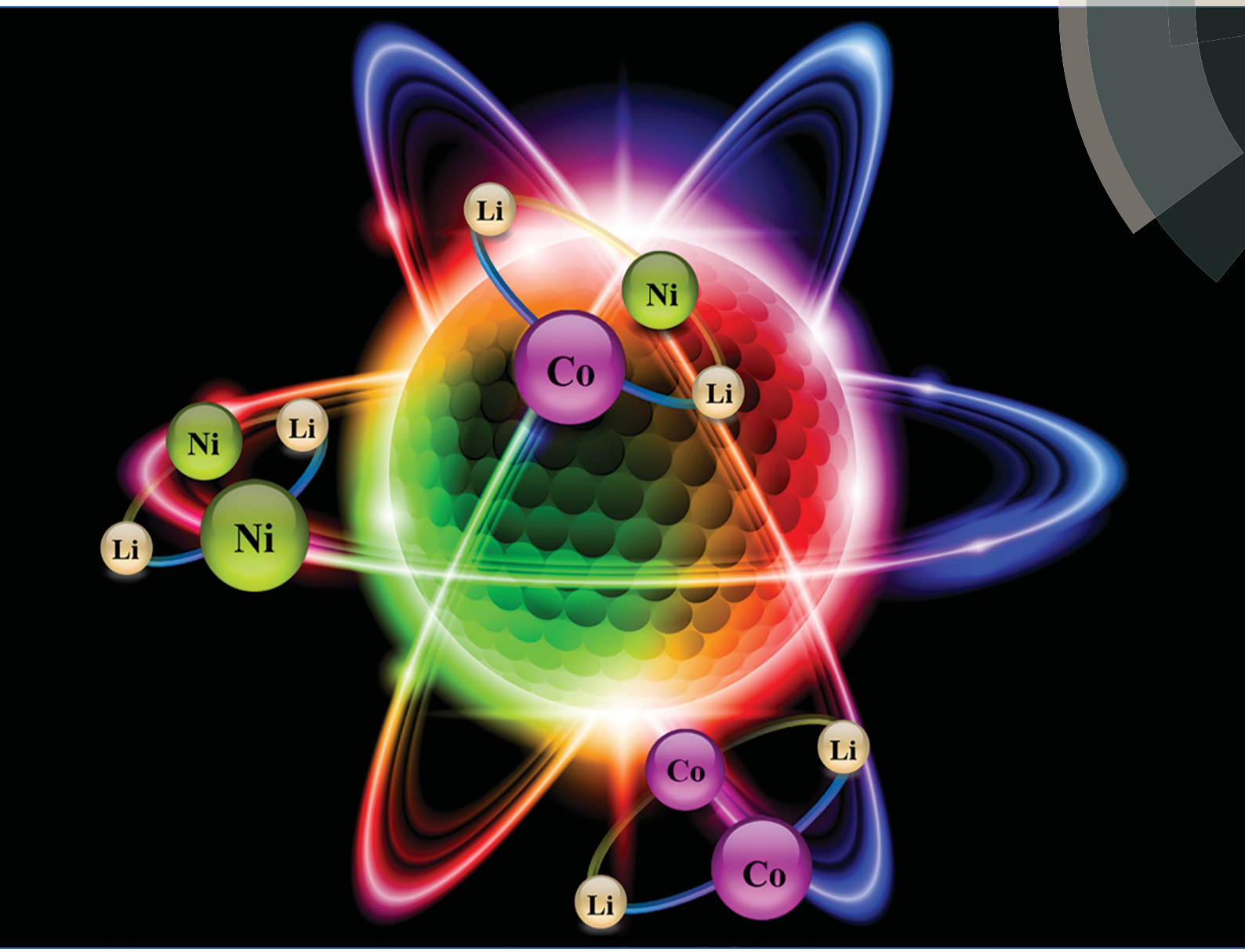

ISSN 2041-6539

ROYAL SOCIETY OF CHEMISTRY

EDGE ARTICLE

Evgeny V. Dikarev *et al.*

A three body problem: a genuine heterotrimetallic molecule *vs.* a mixture of two parent heterobimetallic molecules

Chemical Science

EDGE ARTICLE

View Article Online
View Journal | View Issue

Check for updates

Cite this: *Chem. Sci.*, 2018, **9**, 4736

A three body problem: a genuine hetero*tri*metallic molecule *vs.* a mixture of two parent hetero*bi*metallic molecules†

Haixiang Han,[a] Zheng Wei,[a] Matthew C. Barry,[a] Jesse C. Carozza,[a] Melisa Alkan,[b] Andrey Yu Rogachev,[b] Alexander S. Filatov,[c] Artem M. Abakumov[d] and Evgeny V. Dikarev *[a]

This work raises a fundamental question about the "real" structure of molecular compounds containing three different metals: whether they consist of genuine hetero*tri*metallic species or of a mixture of parent hetero*bi*metallic species. Heterotrimetallic complex $Li_2CoNi(tbaoac)_6$ (**1**, tbaoac = *tert*-butyl acetoacetate) has been designed based on the model tetranuclear structure featuring two transition metal sites in order to be utilized as a molecular precursor for the low-temperature preparation of the $LiCo_{0.5}Ni_{0.5}O_2$ battery cathode material. An investigation of the structure of **1** appeared to be very challenging, since the Co and Ni atoms have very similar atomic numbers, monoisotopic masses, and radii as well as the same oxidation state and coordination number/environment. Using a statistical analysis of heavily overlaid isotope distribution patterns of the $[Li_2MM'L_5]^+$ (M/M′ = Co_2, Ni_2, and CoNi) ions in DART mass spectra, it was concluded that the reaction product **1** contains both heterotrimetallic and bimetallic species. A structural analogue approach has been applied to obtain $Li_2MMg(tbaoac)_6$ (M = Co (**2**) and Ni (**3**)) complexes that contain lighter, diamagnetic magnesium in the place of one of the 3d transition metals. X-ray crystallography, mass spectrometry, and NMR spectroscopy unambiguously confirmed the presence of three types of molecules in the reaction mixture that reaches an equilibrium, $Li_2M_2L_6 + Li_2Mg_2L_6 \leftrightarrow 2Li_2MMgL_6$, upon prolonged reflux in solution. The equilibrium mixture was shown to have a nearly statistical distribution of the three molecules, and this is fully supported by the results of theoretical calculations revealing that the stabilization energies of hetero*tri*metallic assemblies fall exactly in between those for the parent hetero*bi*metallic species. The $LiCo_{0.5}Ni_{0.5}O_2$ quaternary oxide has been obtained in its phase-pure form by thermal decomposition of heterometallic precursor **1** at temperatures as low as 450 °C. Its chemical composition, structure, morphology, and transition metal distribution have been studied by X-ray and electron diffraction techniques and compositional energy-dispersive X-ray mapping with nanometer resolution. The work clearly illustrates the advantages of heterometallic single-source precursors over the corresponding multi-source precursors.

Received 26th February 2018
Accepted 5th May 2018

DOI: 10.1039/c8sc00917a

rsc.li/chemical-science

Open Access Article. Published on 08 May 2018. Downloaded on 12/9/2025 5:14:29 AM.
This article is licensed under a Creative Commons Attribution-NonCommercial 3.0 Unported Licence.

Introduction

The rapid development of energy-related materials has brought about a great need for new design strategies to improve their performance.[1–4] It is well known that the properties of materials, such as their electrochemical, catalytic, or magnetic properties, are closely related to the status of 3d transition metals in the host structure.[5–11] The advance of compounds that incorporate two or more different transition metals has been primarily achieved on the basis of the well-established single-transition-metal-containing archetypes[12–14] and has significantly expanded the research field of both new materials and modified known phases.[15–18] Since the transition metal–oxygen framework typically holds the key to the overall structure type, each single transition metal is capable of endowing compounds with unique properties.[19–21] At the same time, the combination of different 3d transition metals affords the materials with overall more balanced properties, while compensating for the drawbacks brought about by individual metals as well.[22,23] Moreover, variables such as transition metal types and ratios are extra parameters that allow one to subtly tune the properties of target

[a]*Department of Chemistry, University at Albany, SUNY, Albany, NY 12222, USA. E-mail: edikarev@albany.edu*

[b]*Department of Chemistry, Illinois Institute of Technology, Chicago, IL 60616, USA*

[c]*Department of Chemistry, The University of Chicago, IL 60637, USA*

[d]*Center for Electrochemical Energy Storage, Skolkovo Institute of Science and Technology, Moscow 143026, Russia*

† Electronic supplementary information (ESI) available: Experimental procedures, synthetic details, X-ray powder diffraction patterns, IR and mass spectra, phase analysis of thermal decomposition traces of the heterometallic precursor. CCDC 1823874–1823877. For ESI and crystallographic data in CIF or other electronic format see DOI: 10.1039/c8sc00917a

This journal is © The Royal Society of Chemistry 2018

Open Access Article. Published on 08 May 2018. Downloaded on 12/9/2025 5:14:29 AM.
This article is licensed under a Creative Commons Attribution-NonCommercial 3.0 Unported Licence.

materials based on specific needs.[24–27] Among the numerous cases showing the benefits of combining two different 3d transition metals, there is an interesting $LiCo_{0.5}Ni_{0.5}O_2$ oxide that is considered as a cathode material for lithium-ion batteries.[1,6,28,29] By substituting a half portion of Co with Ni in $LiCoO_2$ (LCO), this layered phase has been found to be superior to both corresponding ternary oxides by demonstrating higher capacity and reversibility over cycling.[22,29–32]

One of the biggest challenges in the preparation of materials containing two or more 3d transition metals is that synthetic methods are typically limited to conventional solid state reactions.[7,17,33–35] Preparation of stoichiometric trimetallic oxides like $LiCo_{0.5}Ni_{0.5}O_2$ usually requires harsh synthetic conditions, *e.g.* high calcination temperatures and long annealing times.[22,28,31,33] Such synthetic routes impose difficulties for manipulating nanostructured particles with a narrow size distribution and often cause the loss of Li resulting in the appearance of nonstoichiometric impurities like the Ni-rich $Li_xNi_{2-x}O_2$ ($0 < x < 1$).[20,29,30] In addition, an irregular morphology and inhomogeneous chemical composition/transition metal distribution are commonly encountered problems,[36,37] especially when certain thermodynamically favoured binary oxides are formed during the synthetic process.[37–39]

One of the ways to avoid the above problems is the application of single-source precursors (SSPs) – molecules containing all the necessary metals in an appropriate ratio and decomposable in a controllable manner under mild conditions to yield phase-pure target materials.[40–43] Single-source precursors having an intimate mixing of elements at the molecular level undergo a clean low-temperature thermolysis to produce nanomaterials with a homogeneous metal distribution throughout the product, as a result of rapid interactions between constituent elements, and reduce the possibility of generating unwanted intermediates.[41,44–46]

The design of a hetero*tri*metallic molecular precursor for the $LiCo_{0.5}Ni_{0.5}O_2$ oxide material is not a trivial task. It requires, at least, a tetranuclear molecule containing Li, Co, and Ni in a 2 : 1 : 1 ratio. We proposed to utilize hetero*bi*metallic analogue $Li_2M_2L_6$, which is a tetranuclear cyclic molecule (Scheme 1) with two transition metal sites. Molecules of that type were shown to be readily prepared on a large scale and to be capable of accommodating a number of divalent metals that prefer an octahedral environment, including even main group metals like Mg.[41,47] Construction of such cyclic molecules requires the utilization of unsymmetric ligands (diketonates and beta-ketoesters) that feature different (small/bulky) substituents at the two ligand ends. The ligand oxygen located under small (CH_3, CF_3) substituents acts as a chelating–bridging, while the other one, under bulky (O^{t}Bu, ^{t}Bu) groups, is purely chelating. The bulky ligand tails face outward of the heterometallic assembly and prevent further oligomerization of the metal core, ensuring an impressive stability of $Li_2M_2L_6$ molecules in the solid state, gas phase, and solution. Importantly, the above hetero*bi*metallic precursors proved to be efficient in producing phase-pure $LiMO_2$ layered oxides, with L = tbaoac (*tert*-butyl acetoacetate; R = Me, R′ = O^{t}Bu) leading the way as the most efficient ligand for clean, low-temperature decomposition.

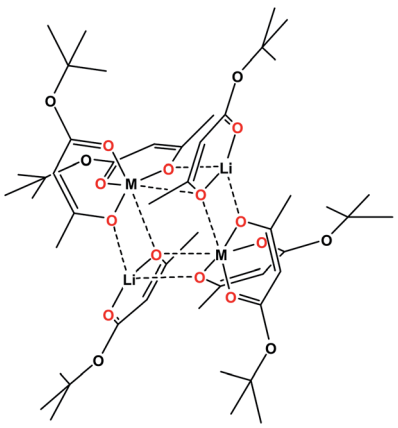

Scheme 1

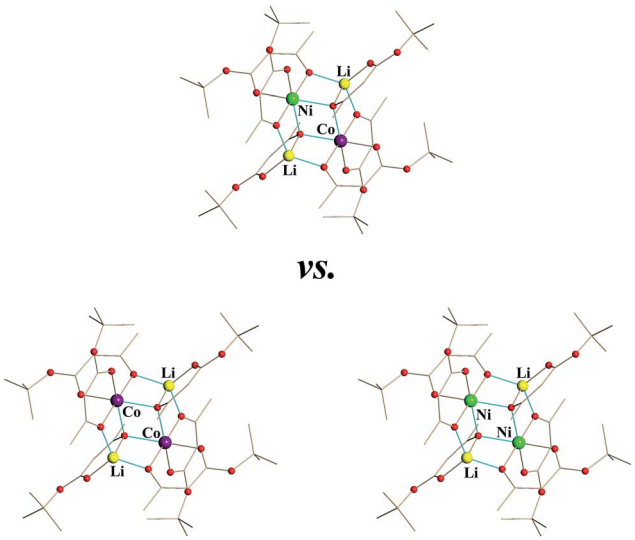

Scheme 2

In this work, we have successfully employed the model tetranuclear structure (Scheme 1) to obtain hetero*tri*metallic precursor $Li_2CoNi(tbaoac)_6$ (**1**), which was successfully utilized to produce the phase-pure target oxide $LiCo_{0.5}Ni_{0.5}O_2$ upon low-temperature thermolysis. Despite this accomplishment, our research has raised a fundamental issue regarding the structure of hetero*tri*metallic precursor **1**: whether it consists of genuine hetero*tri*metallic molecules or contains a statistical mixture of two hetero*bi*metallic units (Scheme 2). Herein we describe our approaches to decode the structure of such hetero*tri*metallic molecules in what can perhaps be regarded as one of the most complex cases.

Hetero*tri*metallic precursor $Li_2CoNi(tbaoac)_6$ (1)

Synthesis and properties

Hetero*tri*metallic precursor $Li_2CoNi(tbaoac)_6$ (**1**) was prepared by routes represented by eqn (1) and (2). Both reactions can be

Open Access Article. Published on 08 May 2018. Downloaded on 12/9/2025 5:14:29 AM.
This article is licensed under a Creative Commons Attribution-NonCommercial 3.0 Unported Licence.

run in the solid state or in solution and employ commercially/readily available starting reagents. The solution approach affords the product on a large scale, in nearly quantitative yield (see the ESI† for full synthetic details). The first preparative technique (eqn (1)) is a one-step reaction of anhydrous transition metal(II) chlorides with an excess of Li(tbaoac). The heterometallic product is readily separable from LiCl based on their different solubilities in dichloromethane. The second technique represents a stoichiometric addition of homometallic lithium and divalent transition metal tbaoac salts and is performed in non-coordinating solvents such as 1,2-dichloroethane (DCE). While this reaction affords the heterometallic precursor as the sole product, it requires the preparation of $M(tbaoac)_2$ complexes as an additional step. Synthetic conditions such as solvent, temperature, and time were shown to have a significant influence on the composition of the final product (*vide infra*).

$$6Li(tbaoac) + CoCl_2 + NiCl_2 \rightarrow Li_2CoNi(tbaoac)_6 + 4LiCl \quad (1)$$

$$2Li(tbaoac) + Co(tbaoac)_2 + Ni(tbaoac)_2 \rightarrow Li_2CoNi(tbaoac)_6 \quad (2)$$

Hetero*tri*metallic precursor **1** was isolated in the form of fine crystalline powder. It can be further purified by sublimation in dynamic vacuum (cold finger) at 140–160 °C. The absence of crystalline impurities in the bulk sample of **1** was confirmed by comparison of its experimental X-ray powder pattern with the one calculated from the single crystal data (ESI, Fig. S2 and Table S5†). ICP-MS analysis of the reaction product provided the ratio of Co : Ni as 0.51(1) : 0.49(1). The product displays a homogeneous brown colour distribution that is clearly different from both pure hetero*bi*metallic $Li_2Co_2(tbaoac)_6$ (purple) and $Li_2Ni_2(tbaoac)_6$ (green). Compound **1** cannot be sublimed at the static vacuum conditions (sealed, evacuated glass ampule), which is strikingly different from the behaviour of $Li_2Co_2(tbaoac)_6$, which is volatile at 140 °C under the same conditions. The other properties of **1** are very similar to those of the parent hetero*bi*metallic complexes: it can be quantitatively resublimed under dynamic vacuum without any visible indications of differently coloured components, it is highly soluble in all common solvents, and stable in open air for a reasonable period of time. In addition, the crystals of **1**, regardless of growing conditions, always appear as allotwins[48] consisting of triclinic and monoclinic polytypes that differ by mutual packing of the $Li_2M_2L_6$ molecules (ESI, Fig. S2†).

Crystal structure

Single crystal X-ray investigation of hetero*tri*metallic precursor **1** revealed that its tetranuclear structure (Fig. 1) is isomorphous to both hetero*bi*metallic $Li_2Co_2(tbaoac)_6$ and $Li_2Ni_2(tbaoac)_6$. It conforms to the centrosymmetric triclinic space group with an inversion centre located in the middle of the heterometallic assembly. Thus, only a single transition metal position is crystallographically independent. Unsurprisingly, the refinement of this position as 50 : 50 Co/Ni as well as pure Co or Ni did not result in an alteration of the *R*-value, standard deviations, or

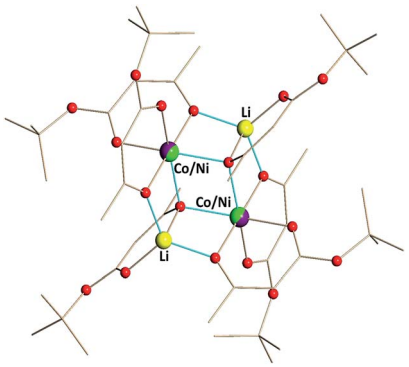

Fig. 1 Solid state structure of $Li_2CoNi(tbaoac)_6$ (**1**). The lithium–oxygen and transition metal–oxygen bonds to the tbaoac ligands involved in the bridging interactions are shown in blue. Hydrogen atoms are omitted for clarity. The full view of the structure drawn with thermal ellipsoids can be found in ESI, Fig. S6.†

thermal parameters beyond statistically significant values (ESI, Table S12†). Careful inspection of the M–O bond distances in the structure of **1** indicates that the lengths of all three different types of interactions (chelating, chelating–bridging, and bridging) fall in between the corresponding characteristics established for the Co–O and Ni–O bonds in hetero*bi*metallic analogues (Table 1).

An analysis of the structural features in **1** brings up an important question: does the structure of the trimetallic product consist only of hetero*tri*metallic $Li_2CoNi(tbaoac)_6$ molecules in their alternative orientations or does it contain a statistical mixture of hetero*bi*metallic $Li_2Co_2(tbaoac)_6$ and $Li_2Ni_2(tbaoac)_6$ assemblies (Scheme 3). In terms of the application aspect, the query can be formulated as follows: does the heterometallic compound represent a single-source or a multi-source precursor?

This is a common problem that should be accounted for in any heteromultimetallic molecule, especially when two of its metal atoms have the same oxidation state and coordination number/environment as well as very similar radii and atomic numbers/masses. The situation becomes even more complicated in the case when there is an extra symmetry within the molecule, and the metal atoms in question are not crystallographically independent. Apparently, other diffraction methods such as neutron and resonant diffraction that we have successfully applied before[49] for analysis of site occupancy by 3d transition metal atoms cannot resolve the above problem, other than to confirm mixed-occupancy and to provide "elemental

Table 1 Averaged metal–oxygen bond distances (Å) in the structures of heterometallic precursors. The full list of bond distances and angles can be found in ESI, Table S11

	M–O_c[a]	M–O_{c-b}[b]	M–O_b[c]	Li–O
$Li_2Co_2(tbaoac)_6$	2.062(2)	2.028(2)	2.160(2)	1.897(4)
$Li_2Ni_2(tbaoac)_6$	2.016(1)	2.005(1)	2.131(1)	1.886(2)
$Li_2CoNi(tbaoac)_6$ (**1**)	2.038(1)	2.015(1)	2.147(1)	1.894(2)

[a] c – chelating. [b] c–b – chelating–bridging. [c] b – bridging.

This journal is © The Royal Society of Chemistry 2018

Open Access Article. Published on 08 May 2018. Downloaded on 12/9/2025 5:14:29 AM.
This article is licensed under a Creative Commons Attribution-NonCommercial 3.0 Unported Licence.

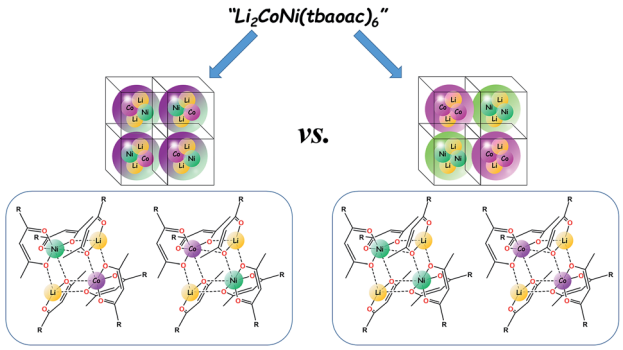

Scheme 3

analysis" data for a particular single crystal. Thus we turned to mass spectrometry in order to analyse the composition of heterometallic molecules based on the rich isotope distribution patterns of accessible mother ions.

Mass spectrometry investigation

DART (Direct Analysis in Real Time) mass spectrometry has already been established as a powerful tool for investigating the gas phase behaviour of volatile heterometallic compounds[42,43,47] as well as for confirmation of transition metal oxidation states.[49] In this work, we extended the application scope of the technique for analysis of hetero*tri*metallic compounds primarily based on their isotope distribution patterns. In accord with their heterocyclic tetranuclear structure, the title molecules exhibit high volatility along with a sufficiently large temperature window between sublimation and decomposition, as well as sound structural stability upon retaining the heterometallic assembly in the gas phase.

In the positive mode mass spectra of hetero*tri*metallic precursor **1**, the $[M–L]^+$ ($M = Li_2M'_2L_6$; M'_2 = CoNi, Co_2, and Ni_2; L = tbaoac) ion appears as a dominant peak. Analysis of the $[M–L]^+$ ion isotope distribution pattern can provide a basis for recognition of molecular $Li_2Co_2(tbaoac)_6$, $Li_2Ni_2(tbaoac)_6$, and $Li_2CoNi(tbaoac)_6$ species that might be present in the bulk hetero*tri*metallic product. Unfortunately, the severe overlap in the isotope distribution patterns (Table 2) of the three possible $[M–L]^+$ ions makes the quantitative analysis quite problematic.

Despite the observed overlap, a careful examination of the isotope distribution pattern "shape" in the mass spectrum of precursor **1** obtained by the above-described reaction (eqn (2)) at room temperature enabled us to make an important conclusion:

Table 2 Relative abundance (%) of the five most intense $[M–L]^+$ isotope peaks in simulated spectra of the $[L_2M'_2L_5]^+$ (M'_2 = Co_2, Ni_2, and Co/Ni) ions

m/*z*	$[Li_2Co_2L_5]^+$	$[Li_2Ni_2L_5]^+$	$[Li_2CoNiL_5]^+$
915		100.0%	15.5%
916	15.6%	55.2%	100%
917	55.2%	89.6%	43.3%
918	100%	49.4%	51.0%
919	12.3%	40.0%	21.8%

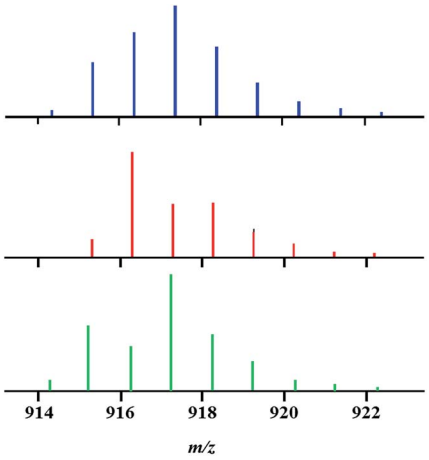

Fig. 2 Isotope distribution patterns for the $[M–L]^+$ ions in the mass spectra of bulk product **1** (experimental, top); $[Li_2CoNiL_5]^+$ (calculated, middle); and an equimolar mixture of $Li_2Co_2L_6$ and $Li_2Ni_2L_6$ complexes (experimental, bottom).

it represents a mixture of hetero*tri*metallic and both hetero-*bi*metallic ions. Indeed, the experimental isotope distribution pattern (Fig. 2) matches neither the calculated profile for pure trimetallic $[Li_2CoNiL_5]^+$ ions, nor the one for a mixture of bimetallic $[Li_2Co_2L_5]^+$/$[Li_2Ni_2L_5]^+$ ions taken in any ratio.

Having this important conclusion established on a qualitative level, we attempted to analyse mass spectra for quantification of three $[M–L]^+$ ions in four major samples (Fig. 3): (a) an equimolar physical mixture of hetero*bi*metallic $Li_2Co_2(tbaoac)_6$ and $Li_2Ni_2(tbaoac)_6$ complexes dissolved in 1,2-dichloroethane (DCE) at room temperature; (b) product **1** obtained from the stoichiometric reaction of Li, Co, and Ni tbaoac complexes (eqn (2)) in DCE at room temperature for 24 h; (c) the same reaction performed in DCE at reflux conditions for 24 h; and (d) reflux of the reaction mixture in DCE for 2 weeks. Five high-

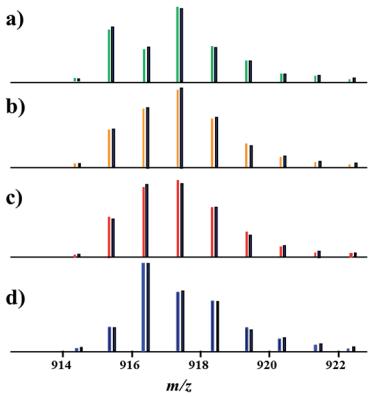

Fig. 3 Isotope distribution patterns for the $[M–L]^+$ (L = tbaoac) ions in positive ion DART mass spectra: (a) an equimolar mixture of hetero-*bi*metallic $Li_2M_2(tbaoc)_6$ (M_2 = Co_2 and Ni_2) complexes; (b) initial reaction (eqn (2)) in DCE at room temperature for 24 h; (c) reflux in DCE for 24 h; and (d) reflux in DCE for 2 weeks. The black lines are simulated isotope distribution patterns that were calculated based on the ratios of $[Li_2Co_2L_5]^+$, $[Li_2Ni_2L_5]^+$, and $[Li_2CoNiL_5]^+$ species shown in Table 3.

Open Access Article. Published on 08 May 2018. Downloaded on 12/9/2025 5:14:29 AM.
This article is licensed under a Creative Commons Attribution-NonCommercial 3.0 Unported Licence.

Table 3 Percentage ratios of individual $[M–L]^+$ ions obtained from the simulated overlaid isotope distribution patterns

	$[Li_2Ni_2L_5]^+$	$[Li_2CoNiL_5]^+$	$[Li_2Co_2L_5]^+$
(a)	61%	0	39%
(b)	38%	38%	24%
(c)	34%	44%	22%
(d)	17%	72%	11%

intensity peaks with m/z = 915, 916, 917, 918, and 919 were utilized to calculate the individual ion ($[Li_2Co_2L_5]^+$, $[Li_2Ni_2L_5]^+$, and $[Li_2CoNiL_5]^+$) percentage ratios (Table 3).

The calculations revealed a clear trend in the relative intensities of the three ions upon changing the reaction conditions. Thus, an equimolar mixture of parent Li_2Co_2(tbaoac)$_6$ and Li_2Ni_2(tbaoac)$_6$ complexes in DCE (Fig. 3a) yields an isotope distribution pattern that can be described by the presence of only $[Li_2Ni_2L_5]^+$ and $[Li_2Co_2L_5]^+$ ions in a ratio of 61 : 39, indicating no interaction between hetero*bi*metallic molecules at such conditions. It also rules out any "recombination reactions" taking place in the mass spectrometer, and so all other spectra were recorded at exactly the same conditions. As we have already mentioned, the mass spectrum of **1** obtained by the reaction (eqn (2)) in DCE at room temperature (Fig. 3b) contains both hetero*tri*metallic $[Li_2CoNiL_5]^+$ and hetero*bi*metallic $[Li_2Ni_2L_5]^+$ and $[Li_2Co_2L_5]^+$ species, whose abundances were calculated to be 38 : 38 : 24. Running the same reaction at reflux conditions increases the content of hetero*tri*metallic ions to 44% (Fig. 3c). Apparently, the scrambling takes place and the content of the target Li_2CoNi(tbaoac)$_6$ molecules keeps growing upon extending the reaction time. After a two week reflux of the reaction mixture in DCE, the percentage of the hetero*tri*metallic $[Li_2CoNiL_5]^+$ ion in the mass spectrum gradually reaches its maximum at 72% (Fig. 3d) and does not grow any further despite elevating the temperature by using higher boiling solvent.

It should be underlined that the relative percentage ratio of ions extracted from the DART-MS data does not directly represent the actual molar ratio of the corresponding parent molecules in the solid sample, since their appearance is highly influenced by many factors, the most important of them being volatility, ionization, and the gas phase thermal stability. Notably, in all four spectra, regardless of the sample preparation conditions, the intensity ratio of $[Li_2Ni_2L_5]^+/[Li_2Co_2L_5]^+$ ions is consistently about 3 : 2, while any of the solid samples under investigation should contain equimolar amounts of Li_2Ni_2(tbaoac)$_6$ and Li_2Co_2(tbaoac)$_6$ molecules.

The structural analogue approach

Design of structural analogues

Analysing the structure and composition of hetero*tri*metallic products like Li_2CoNi(tbaoac)$_6$ (**1**) proved to be a very complicated task as (i) Co and Ni have similar atomic numbers and radii, and therefore, they cannot be distinguished by X-ray diffraction, especially in the case of mixed-occupancy; (ii) very similar monoisotopic masses of cobalt and nickel (58.9332 and 57.9353, respectively) result in a severe overlap of the isotope distribution patterns for the $[M–L]^+$ ions; and (iii) both divalent metal ions are high-spin, thus preventing the use of NMR spectroscopy for characterization of tetranuclear molecules in solution.

Considering all these issues, a structural analogue strategy was adopted in order to rationalize the trends in the formation of hetero*tri*metallic assemblies. We proposed to replace one of the 3d transition metals with another element that (i) in its +2 oxidation state exhibits the same coordination behaviour as Co and Ni to ensure no changes in the connectivity pattern within the tetranuclear Li_2M_2(tbaoac)$_6$ assembly; (ii) has an atomic number that is different enough from Co and Ni to be unambiguously distinguished by X-ray diffraction analysis; (iii) has a monoisotopic mass sufficiently different from those of Co and Ni in order to eliminate the possible overlap of hetero*bi*- and hetero*tri*metallic ions in the mass spectra; (iv) is diamagnetic, so that the presence of its hetero*bi*metallic $Li_2M_2L_6$ molecules in solution can be detected by multinuclear NMR spectroscopy.

After an extensive search for the most appropriate metal, we settled on magnesium as the best (though not ideal) candidate fulfilling the above requirements in order to allow an investigation into the formation and structure of hetero*tri*metallic compounds Li_2MMg(tbaoac)$_6$ (M = Co or Ni). Magnesium was found to support the tetranuclear type of structure $Li_2Mg_2L_6$ with a number of unsymmetric ligands, all isomorphous to those of 3d transition metals.[47] Divalent Mg can be neither reduced nor oxidized in the presence of divalent Ni and Co. Its atomic number and monoisotopic mass (23.9850) are far from those of the 3d transition metals of interest. Finally, the Li_2Mg_2(tbaoac)$_6$ molecule has been thoroughly characterized[47] in solutions of non-coordinating solvents by multinuclear NMR spectroscopy.

Synthesis and structure of the Mg-containing analogues

Hetero*tri*metallic compounds Li_2CoMg(tbaoac)$_6$ (**2**) and Li_2NiMg(tbaoac)$_6$ (**3**) have been prepared with nearly quantitative yields by the reactions described above for the synthesis of Li_2CoNi(tbaoac)$_6$ (**1**) (see the ESI† for more details). Compounds **2** and **3** appear very similar to the parent hetero*bi*metallic complexes in terms of crystal shape, solubility, and thermal stability. They have almost the same colour as the corresponding Co and Ni complexes, but not as the Mg one, which is colourless. The only obvious difference is the volatility of compound **2**, which cannot be sublimed in a sealed evacuated ampule as its dicobalt counterpart.

Single crystal X-ray diffraction investigation confirmed that both Li_2MMg(tbaoac)$_6$ compounds (M = Co (**2**) and Ni (**3**)) are indeed the structural analogues of Li_2CoNi(tbaoac)$_6$ (**1**) as well as of the parent hetero*bi*metallic complexes. That was expected, since the Mg–O distances in the structure of Li_2Mg_2(tbaoac)$_6$ are similar to those of Co–O and Ni–O. Perhaps, this is one of the major reasons why magnesium is able to support the title tetranuclear structure. As of today, we were unable to find the divalent metal that readily forms the $Li_2M_2L_6$ structure while

 This journal is © The Royal Society of Chemistry 2018

Open Access Article. Published on 08 May 2018. Downloaded on 12/9/2025 5:14:29 AM.
This article is licensed under a Creative Commons Attribution-NonCommercial 3.0 Unported Licence.

exhibiting M–O distances that are significantly different from those of 3d transition metals (Mn–Zn). The metal–oxygen distances in **2** and **3** predictably fall within the range established for the parent $Li_2M_2(tbaoac)_6$ (M_2 = Co_2, Ni_2, and Mg_2) molecules (ESI, Table S15†). However, in the case of Mg-containing compounds **2** and **3** (Fig. 4), a mixed occupancy in the sole crystallographically independent metal position has been successfully refined resulting in M : Mg ratios of 53 : 47 (M = Co) and 47 : 53 (M = Ni). Several single crystals taken from the same batch typically gave M : Mg ratios within 3% of 50 : 50. The largest deviations from parity (up to Ni : Mg = 41 : 59) are characteristic of the crystals grown from the bulk product that was obtained by the reactions at room temperature, while those derived from the compounds prepared at long-time reflux conditions show M : Mg ratios closer to 1 : 1. The departure from an ideal composition is reflective of the fact that compounds **2** and **3** do not consist of hetero*tri*metallic $Li_2MMg(tbaoac)_6$ molecules alone. The deviations result from the differences (even small) in solubilities of hetero*bi*metallic molecules $Li_2Mg_2(tbaoac)_6$ and $Li_2M_2(tbaoac)_6$.

Mass spectrometry investigation of Mg-containing analogues

DART mass spectrometry has provided unambiguous evidence for the concomitant presence of hetero*tri*metallic $Li_2MMg(tbaoac)_6$ (M = Co or Ni) and hetero*bi*metallic parent compounds $Li_2M_2(tbaoac)_6$ and $Li_2Mg_2(tbaoac)_6$ in the structural analogue products **2** and **3**. As can be seen from Fig. 5, physical mixtures of heterobimetallic complexes $Li_2M_2(tbaoac)_6$ and $Li_2Mg_2(tbaoac)_6$ give only bimetallic $[Li_2M_2L_5]^+$ peaks with no trimetallic $[Li_2MMg(tbaoac)_5]^+$ counterparts present. The latter clearly appear in the spectra of products obtained in the reaction described by eqn (2) in DCE at room temperature. Now, three ions $[Li_2Mg_2L_5]^+$, $[Li_2MMgL_5]^+$, and $[Li_2M_2L_5]^+$ (M = Co or Ni) show up in the spectra without any overlap. In both cases, the relative intensity of hetero*tri*metallic $[LiMMgL_5]^+$ peaks increases obviously upon increasing the reaction temperature and time. Similar to the case of $Li_2CoNi(tbaoac)_6$ (**1**), the intensities of the $[LiMMgL_5]^+$ peaks reach their maximum at 51% and 50% for the Co- and Ni-containing compounds, respectively, after two weeks of reflux in DCE and exhibit no further meaningful progression after that point, thus indicating that the equilibrium $Li_2M_2(tbaoac)_6 + Li_2Mg_2(tbaoac)_6 \leftrightarrow 2Li_2MMg(tbaoac)_6$ has been established. As we have mentioned earlier in the case of compound **1**, the intensity ratios of $[Li_2Mg_2L_5]^+/[Li_2M_2L_5]^+$ ions in all four spectra are almost the same at *ca.* 1.3 and 1.6 for M = Co and Ni, respectively. An estimation of the molar content of hetero*tri*metallic species in the reaction mixture at equilibrium gives 51% and 50% for products **2** and **3**, respectively.

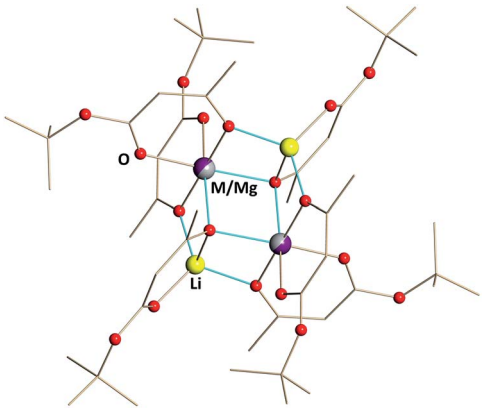

Fig. 4 Solid state structure of $Li_2MMg(tbaoac)_6$ (M = Co (**2**) and Ni (**3**)) products. The metal–oxygen bonds involved in the bridging interactions are shown in blue. Hydrogen atoms are omitted for clarity. The full views of the structures drawn with thermal ellipsoids as well as the bond distances can be found in ESI, Fig. S7 and S8, and Tables S13 and S14.†

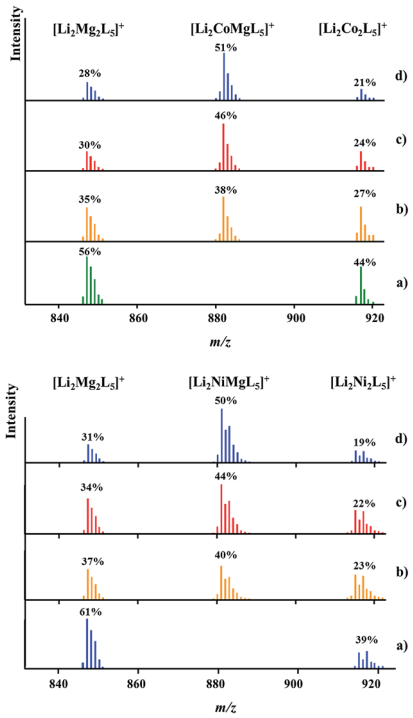

Fig. 5 Isotope distribution patterns for the $[Li_2MMgL_5]^+$ ions in the positive ion DART mass spectra of $Li_2CoMg(tbaoac)_6$ (**2**, top) and $Li_2NiMg(tbaoac)_6$ (**3**, bottom) products: (a) an equimolar mixture of hetero*bi*metallic $Li_2M_2(tbaoc)_6$ (M = Co or Ni) and $Li_2Mg_2(tbaoac)_6$ complexes; (b) initial reaction (eqn (2)) in DCE at room temperature for 24 h; (c) reflux in DCE for 24 h; and (d) reflux in DCE for 2 weeks. The intensity percentages were calculated based on the monoisotopic masses of the corresponding ions.

^{1}H NMR investigation of structural analogue $Li_2NiMg(tbaoac)_6$ (3)

One of the reasons behind selecting magnesium to design the structural analogues of the $Li_2CoNi(tbaoac)_6$ (**1**) complex was the prospect of using NMR spectroscopy in order to unambiguously confirm/disprove the presence of diamagnetic $Li_2Mg_2(tbaoac)_6$ molecules in the products and to estimate the molar ratio (as well as its change based on synthetic conditions) of hetero*bi*metallic and hetero*tri*metallic molecules in the reaction mixture.

Open Access Article. Published on 08 May 2018. Downloaded on 12/9/2025 5:14:29 AM.
This article is licensed under a Creative Commons Attribution-NonCommercial 3.0 Unported Licence.

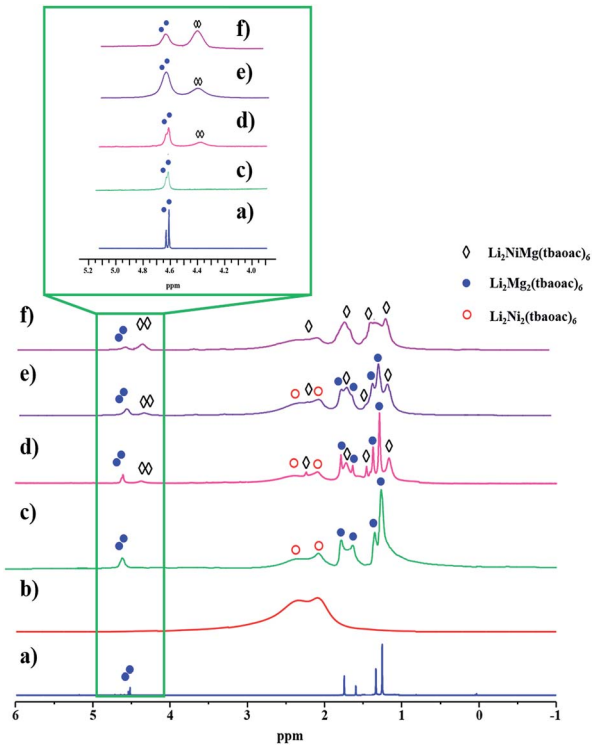

Fig. 6 ^{1}H NMR spectra of heterometallic tetranuclear complexes in $CDCl_3$ recorded at room temperature: (a) $Li_2Mg_2(tbaoac)_6$; (b) $Li_2Ni_2(tbaoac)_6$; (c) an equimolar mixture of $Li_2Ni_2(tbaoac)_6$ and $Li_2Mg_2(tbaoac)_6$; (d) the product isolated from the initial reaction (eqn (2)) in DCE at room temperature for 24 h; (e) reflux in DCE for 24 h; and (f) reflux in DCE for 2 weeks. The aromatic proton region is shown in the inset.

While the $Li_2CoMg(tbaoac)_6$ (**2**) analogue was found to be nearly impossible to analyse, the Ni-counterpart (**3**) revealed meaningful features in its proton NMR spectra. The ^{1}H NMR spectrum of pure $Li_2Mg_2(tbaoac)_6$ in $CDCl_3$ clearly shows two sets of singlets for C*H*, CH_3 and OC(CH_3)$_3$ protons (*ca.* 1 : 3 : 9), which correspond to the 1 : 2 distribution of tbaoac ligands chelating lithium and magnesium, respectively (Fig. 6a). Importantly, this spectrum provides a basis for understanding the spectral features of the other two participants, $Li_2Ni_2(tbaoac)_6$ and $Li_2NiMg(tbaoac)_6$ (**3**).

While the spectrum of $Li_2Ni_2(tbaoac)_6$ displays just an overlaid "bump" due to the presence of two high-spin divalent nickel centres (Fig. 6b), in the spectrum of an equimolar mixture of hetero*bi*metallic $Li_2Ni_2(tbaoac)_6$ and $Li_2Mg_2(tbaoac)_6$ compounds, some of the visibly broadened proton peaks can be reasonably assigned (Fig. 6c). Compared to the latter spectrum, the one recorded for the bulk product of $Li_2NiMg(tbaoac)_6$ (**3**) synthesized at room temperature clearly shows the extra peaks (Fig. 6d) that can be assigned to the hetero*tri*metallic species. Upon increasing the reaction temperature (Fig. 6e) and time (Fig. 6f), the latter peaks keep growing, while the corresponding signals of $Li_2Mg_2(tbaoac)_6$ become weaker. This trend can be seen at its best for the aromatic C*H* protons (Fig. 6, inset) of $Li_2NiMg(tbaoac)_6$ (**3**) and $Li_2Mg_2(tbaoac)_6$, whose integration ratio changes from *ca.* 0.4 to 2.3 on going from spectrum (d) to (f). Further increase of the reaction temperature and/or time beyond this point does not visibly affect the NMR spectrum, pointing out that the equilibrium $Li_2Ni_2(tbaoac)_6$ + $Li_2Mg_2(tbaoac)_6$ ↔ $2Li_2NiMg(tbaoac)_6$ has been reached. The rough estimation gives an almost statistical distribution with the molar content of hetero*tri*metallic species at equilibrium at about 53.5%. Therefore, the NMR study decidedly supports the results of mass spectrometry investigation of structural analogues **2** and **3**.

Theoretical calculations of the $Li_2MM'(tbaoac)_6$ molecules

Theoretical evaluation of thermodynamic stability of tetranuclear molecules was performed using the B2PLYP-D/TZVP/ZORA approach (see the ESI† for more details) by deconstruction of the $Li_2MM'(tbaoac)_6$ assemblies into monomeric units, namely, Li(tbaoac), M(tbaoac)$_2$, and M′(tbaoac)$_2$. As can be seen from the results listed in Table 4, the stabilization energy for the hetero*tri*metallic $Li_2CoNi(tbaoac)_6$ (**1**) molecule falls exactly in between those for its hetero*bi*metallic counterparts, $Li_2Co_2(tbaoac)_6$ and $Li_2Ni_2(tbaoac)_6$. A similar situation is found for the structural analogue $Li_2NiMg(tbaoac)_6$ (**3**), whose stabilization energy is approximately equal to the average value for two parent molecules. Thus, the calculated thermodynamic stabilization energy gives no preference for hetero*tri*metallic systems over the mixture of hetero*bi*metallic ones. These results support the observation that all three types of species are present in the equilibrium mixture $Li_2M_2(tbaoac)_6$ + $Li_2M'_2(tbaoac)_6$ ↔ $2Li_2MM'(tbaoac)_6$ at a roughly statistical 25 : 25 : 50% distribution of components.

Thermal decomposition of the heterometallic precursor $Li_2CoNi(tbaoac)_6$ (1)

According to X-ray powder diffraction analysis, thermal decomposition of the bulk $Li_2CoNi(tbaoac)_6$ (**1**) product obtained from reflux in DCE for 2 weeks yields a phase-pure layered $LiCo_{0.5}Ni_{0.5}O_2$ oxide at temperatures as low as 450 °C (Fig. 7a). The crystallinity of the residue is greatly improved upon elevating the thermolysis temperature up to 750 °C (Fig. 7b). The unit cell parameters of decomposition residues derived from the Le Bail fit correspond well with the literature data[31] for $LiCo_{0.5}Ni_{0.5}O_2$, while being clearly different from

Table 4 Calculated stabilization energies (kcal mol^{-1}) for hetero*bi*metallic and hetero*tri*metallic (**1** and **3**) tetranuclear molecules

$Li_2MM'(tbaoac)_6$	E (bonding, kcal mol^{-1})
$Li_2Co_2(tbaoac)_6$	−134.11
$Li_2Ni_2(tbaoac)_6$	−149.31
$Li_2CoNi(tbaoac)_6$ (**1**)	−141.75
$Li_2Mg_2(tbaoac)_6$	−147.31
$Li_2NiMg(tbaoac)_6$ (**3**)	−148.35

This journal is © The Royal Society of Chemistry 2018

Open Access Article. Published on 08 May 2018. Downloaded on 12/9/2025 5:14:29 AM.
This article is licensed under a Creative Commons Attribution-NonCommercial 3.0 Unported Licence.

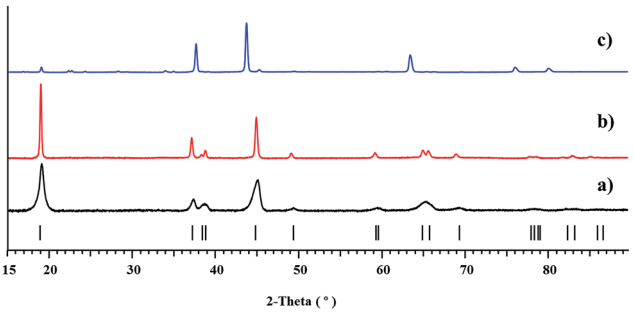

Fig. 7 X-ray powder diffraction patterns of residues obtained by thermal decomposition of (a) the bulk product $Li_2CoNi(tbaoac)_6$ (**1**) at 450 °C and (b) at 750 °C; and (c) an equimolar mixture of $Li_2Co_2(tbaoac)_6$ and $Li_2Ni_2(tbaoac)_6$ at 750 °C. The theoretical peak positions of $LiCo_{0.5}Ni_{0.5}O_2$ oxide are shown at the bottom as black bars.

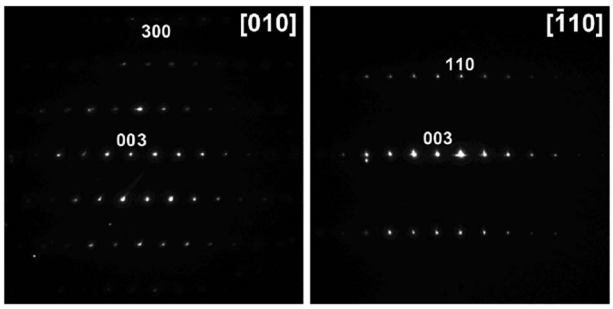

Fig. 8 Electron diffraction patterns of the $LiCo_{0.5}Ni_{0.5}O_2$ residue indexed in the $R\bar{3}m$ space group with unit cell parameters $a \approx 2.8$ and $c \approx 14.1$ Å.

those for the hetero*bi*metallic oxides $LiMO_2$ (M = Co and Ni) (Table 5). Traces of the target oxide material start to appear in the X-ray powder pattern at as low as 350 °C, while the Ni-rich $Li_xNi_{2-x}O_2$ ($0 < x < 1$) phase becomes visible in the samples obtained above 750 °C. Under the same decomposition conditions, the equimolar mixture of hetero*bi*metallic $Li_2Co_2(tbaoac)_6$ and $Li_2Ni_2(tbaoac)_6$ complexes prepared by evaporation of DCE solution at room temperature produces a very complex multi-phase residue (Fig. 7c) that contains nickel-rich $Li_{0.4}Ni_{1.6}O_2$, $LiCoO_2$, and some unidentified compounds (ESI, Fig. S19†). The latter represents an important observation that clearly demonstrates the advantage of single-source precursors over multiple-source precursors.

To the best of our knowledge, 450 °C is the lowest temperature utilized so far to prepare a $LiCo_{0.5}Ni_{0.5}O_2$ material that is free of impurities. The typical solid-state preparative methods for $LiCo_{0.5}Ni_{0.5}O_2$ cathode materials that employ oxides, carbonates, or acetates as starting reagents require high annealing temperatures of *ca.* 700 °C in order to obtain phase-pure materials.[22,28,30,31,50] Several "soft chemistry" routes such as sol–gel[51] as well as other multi-source precursor (assisted precipitation) approaches[29] have also been introduced. While in some of those techniques calcination temperatures as low as 500 °C have been attempted, it was found that the phase-pure $LiCo_{0.5}Ni_{0.5}O_2$ can only be obtained at 600 °C.[29,51]

The X-ray powder diffraction identification of the $LiCo_{0.5}Ni_{0.5}O_2$ oxide phase by its unit cell parameters and the absence of visible crystalline impurities are not enough for thorough characterization of the target material appearance. The morphology of the particles, their chemical composition, and the homogeneous distribution of Co and Ni represent even more important characteristics for practical applications. Therefore, the decomposition residues have been analysed by recording electron diffraction (ED) patterns, high angle annular dark field scanning transmission electron microscopy (HAADF-STEM) images, and energy dispersive X-ray (EDX) spectra. The samples were found to consist of agglomerated crystals with a size of 50–300 nm. The electron diffraction patterns of the oxide phase (Fig. 8) can be indexed in the space group $R\bar{3}m$ with unit cell parameters $a \approx 2.8$ and $c \approx 14.1$ Å, typical of the layered $LiCoO_2$-type structure.[52] EDX compositional maps reveal a predominantly homogeneous distribution of transition metals (Fig. 9) with an averaged Co : Ni atomic ratio of 49.0(16) : 51.0(16). An extensive analysis of electron diffraction images showed some inhomogeneity in the Co/Ni distribution, which was observed only very locally, in the form of small 5–10 nm Ni-enriched (less than 5%) clusters and occasional Co-rich and Co-depleted crystallites (ESI, Fig. S20–S22†). Such

Table 5 Comparison of the unit cell parameters (Å) for the $LiCo_{0.5}Ni_{0.5}O_2$ (Le Bail fit) obtained by the thermal decomposition of heterometallic precursor **1** under different conditions with the literature data for the corresponding quaternary and tertiary oxides

	$LiCo_{0.5}Ni_{0.5}O_2$			$LiCoO_2$	$LiNiO_2$
	450 °C	750 °C	Reported[31]	Reported[49]	Reported[32]
a (Å)	2.8462(2)	2.8474(3)	2.8422(2)	2.8161(5)	2.87549(7)
c (Å)	14.0938(2)	14.0947(2)	14.096(4)	14.0536(5)	14.18056(7)

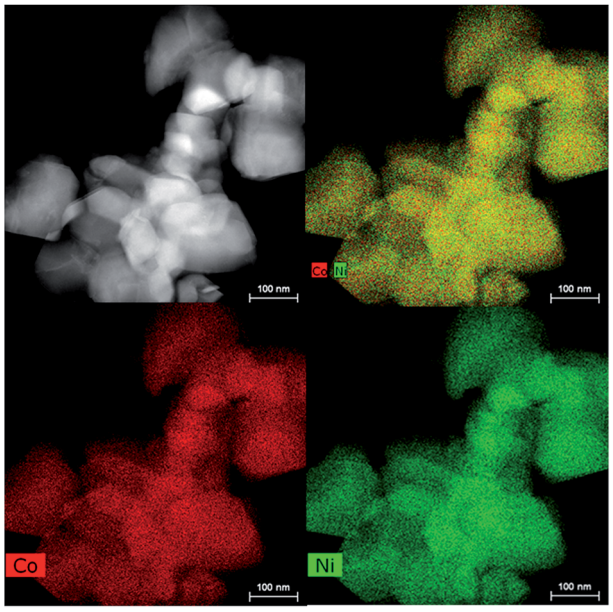

Fig. 9 HAADF-STEM image, the EDX elemental maps for Co, Ni, and O, and the mixed compositional maps showing a homogeneous distribution of Co and Ni in the decomposition residue.

Open Access Article. Published on 08 May 2018. Downloaded on 12/9/2025 5:14:29 AM.
This article is licensed under a Creative Commons Attribution-NonCommercial 3.0 Unported Licence.

inhomogeneity can be attributed to the presence of hetero*bi*metallic molecules $Li_2Co_2(tbaoac)_6$ and $Li_2Ni_2(tbaoac)_6$ in the bulk precursor. Again, this observation clearly underscores the advantages of a single-source precursor over a multi-source precursor.

Conclusions

A hetero*tri*metallic tetranuclear molecular precursor containing two different 3d transition metals, $Li_2CoNi(tbaoac)_6$ (**1**), has been synthesized and successfully applied for the low-temperature preparation of a layered $LiCo_{0.5}Ni_{0.5}O_2$ oxide which is an important cathode material for lithium ion batteries. The work raises a fundamental question regarding the "real" structure of hetero*tri*metallic compounds: do they consist of genuine hetero*tri*metallic species, contain a statistical mixture of two hetero*bi*metallic molecules, or feature all of the above, similar to what was found in this study. We believe that any multimetallic molecule (containing three or more different metals) should be thoroughly analysed taking this point into account.

This study clearly demonstrates the need for the single-source precursor consisting of only hetero*tri*metallic molecules for the preparation of target materials with a perfect homogeneous distribution of metals. The real challenge is how to design such a hetero*tri*metallic molecule that contains at least two different metal atoms with very similar characteristics? We envision two major ways to attain the structural distinctions for such atoms: different oxidation states and/or different coordination environments. In the particular case of the title precursor Li_2CoNiL_6, the former approach translates into making the cationic assembly $[Li_2Co^{III}Ni^{II}L_6]^+$. While this seems to be the most viable synthetic option, two practical points should be taken into account. First, this route will not yield a volatile precursor; instead, it will yield the one that can be applied for bulk or solution decomposition only. Second, a careful consideration of the counteranion chemical composition is required. It should not contain the elements that may affect the purity of decomposition residues, so that several convenient options for anion such as X^-, BF_4^- and PF_6^- are impractical. The second strategy, which involves changing the coordination environment of transition metal centres in the title precursor, implies the application of a mixed-ligand approach. It relies upon using two different ligands with one of them having electron-withdrawing properties to preferentially coordinate the more electron-rich Ni centre, and the other one with electron-donating (or less electron-withdrawing) characteristics to be attached to the Co ion. However, from a practical perspective this approach would likely require as many as three different ligands, since the most electron-donating one will be exclusively located on the Li ion, leaving two transition metals to compete for the rest.

Conflicts of interest

There are no conflicts of interest to declare.

Acknowledgements

Financial support from the National Science Foundation (CHE-1152441) (ED) and from the Illinois Institute of Technology (AR) is gratefully acknowledged. The authors thank CRDF Global (FSCX-16-62133-0, AA) and (OISE-16-62134-0, ED) for funding this collaborative project. ChemMatCARS Sector 15 is principally supported by the Divisions of Chemistry (CHE) and Materials Research (DMR), National Science Foundation, under grant number NSF/CHE-1346572. Use of the PILATUS3 X CdTe 1M detector was supported by the National Science Foundation under grant number NSF/DMR-1531283. Use of the Advanced Photon Source, an Office of Science User Facility operated for the U.S. Department of Energy (DOE) Office of Science by Argonne National Laboratory, was supported by the U.S. DOE under Contract No. DE-AC02-06CH11357.

References

1 M. S. Whittingham, *Chem. Rev.*, 2004, **104**, 4271–4302.
2 J. B. Goodenough, *J. Power Sources*, 2007, **174**, 996–1000.
3 J. B. Goodenough and K.-S. Park, *J. Am. Chem. Soc.*, 2013, **135**, 1167–1176.
4 A. S. Arico, P. Bruce, B. Scrosati, J.-M. Tarascon and W. van Schalkwijk, *Nat. Mater.*, 2005, **4**, 366–377.
5 B. L. Ellis, K. T. Lee and L. F. Nazar, *Chem. Mater.*, 2010, **22**, 691–714.
6 L. Croguennec and M. R. Palacin, *J. Am. Chem. Soc.*, 2015, **137**, 3140–3156.
7 C. Yada, A. Ohmori, K. Ide, H. Yamasaki, T. Kato, T. Saito, F. Sagane and Y. Iriyama, *Adv. Energy Mater.*, 2014, **4**, 1301416.
8 J. Hessels, R. J. Detz, M. T. M. Koper and J. N. H. Reek, *Chem.–Eur. J.*, 2017, **23**, 16413–16418.
9 C. Zheng and S.-L. You, *Chem*, 2016, **1**, 830–857.
10 D. Banham, S. Ye, K. Pei, J.-i. Ozaki, T. Kishimoto and Y. Imashiro, *J. Power Sources*, 2015, **285**, 334–348.
11 S. M. Aldoshin, D. V. Korchagin, A. V. Palii and B. S. Tsukerblat, *Pure Appl. Chem.*, 2017, **89**, 1119–1143.
12 J. C. Knight, S. Therese and A. Manthiram, *J. Electrochem. Soc.*, 2015, **162**, A426–A431.
13 S. Levasseur, M. Menetrier and C. Delmas, *J. Power Sources*, 2002, **112**, 419–427.
14 S. Levasseur, M. Menetrier and C. Delmas, *Chem. Mater.*, 2002, **14**, 3584–3590.
15 P. K. Nayak, E. M. Erickson, F. Schipper, T. R. Penki, N. Munichandraiah, P. Adelhelm, H. Sclar, F. Amalraj, B. Markovsky and D. Aurbach, *Adv. Energy Mater.*, 2017, 1702397.
16 M. Sathiya, K. Hemalatha, K. Ramesha, J. M. Tarascon and A. S. Prakash, *Chem. Mater.*, 2012, **24**, 1846–1853.
17 Y. K. Yoon, C. W. Park, H. Y. Ahn, D. H. Kim, Y. S. Lee and J. Kim, *J. Phys. Chem. Solids*, 2007, **68**, 780–784.
18 K. Saravanan, A. Jarry, R. Kostecki and G. Chen, *Sci. Rep.*, 2015, **5**, 8027.
19 H. Xia, Y. Wan, W. Assenmacher, W. Mader, G. Yuan and L. Lu, *NPG Asia Mater.*, 2014, **6**, e126.

This journal is © The Royal Society of Chemistry 2018

Open Access Article. Published on 08 May 2018. Downloaded on 12/9/2025 5:14:29 AM.
This article is licensed under a Creative Commons Attribution-NonCommercial 3.0 Unported Licence.

20 W. Liu, P. Oh, X. Liu, M.-J. Lee, W. Cho, S. Chae, Y. Kim and J. Cho, *Angew. Chem., Int. Ed.*, 2015, **54**, 4440–4457.
21 M. M. Thackeray, *Prog. Solid State Chem.*, 1997, **25**, 1–71.
22 M. Y. Song, H. Rim and H. R. Park, *Ceram. Int.*, 2013, **39**, 6937–6943.
23 H.-J. Kweon, G. B. Kim, H. S. Lim, S. S. Nam and D. G. Park, *J. Power Sources*, 1999, **83**, 84–92.
24 X. Wang, M. Tamaru, M. Okubo and A. Yamada, *J. Phys. Chem. C*, 2013, **117**, 15545–15551.
25 B. Mortemard de Boisse, D. Carlier, M. Guignard and C. Delmas, *J. Electrochem. Soc.*, 2013, **160**, A569–A574.
26 B. Mortemard de Boisse, PhD thesis, Université de Bordeaux, 2014.
27 F. Zhou, M. Cococcioni, K. Kang and G. Ceder, *Electrochem. Commun.*, 2004, **6**, 1144–1148.
28 S.-J. Lee, J.-K. Lee, D.-W. Kim, H.-K. Baik and S.-M. Lee, *J. Electrochem. Soc.*, 1996, **143**, L268–L270.
29 C. Julien, C. Letranchant, S. Rangan, M. Lemal, S. Ziolkiewicz, S. Castro-Garcia, L. El-Farh and M. Benkaddour, *Mater. Sci. Eng., B*, 2000, **76**, 145–155.
30 I. Belharouak, H. Tsukamoto and K. Amine, *J. Power Sources*, 2003, **119–121**, 175–177.
31 M. V. Reddy, G. V. S. Rao and B. V. R. Chowdari, *J. Phys. Chem. C*, 2007, **111**, 11712–11720.
32 R. Stoyanova, E. Zhecheva, R. Alcántara, J. L. Tirado, G. Bromiley, F. Bromiley and T. Boffa Ballaran, *Solid State Ionics*, 2003, **161**, 197–204.
33 G. X. Wang, J. Horvat, D. H. Bradhurst, H. K. Liu and S. X. Dou, *J. Power Sources*, 2000, **85**, 279–283.
34 J. Cho and B. Park, *J. Power Sources*, 2001, **92**, 35–39.
35 J. M. Wang, J. P. Hu, C. Y. Ouyang, S. Q. Shi and M. S. Lei, *Solid State Commun.*, 2011, **151**, 234–237.
36 P. T. Barton, Y. D. Premchand, P. A. Chater, R. Seshadri and M. J. Rosseinsky, *Chem.–Eur. J.*, 2013, **19**, 14521–14531.
37 E. Antolini and M. Ferretti, *Mater. Lett.*, 1997, **30**, 59–63.
38 E. Antolini, *J. Mater. Chem.*, 1998, **8**, 2783–2786.
39 S. Yang, H. Yue, Y. Yin, J. Yang and W. Yang, *Electrochim. Acta*, 2006, **51**, 4971–4976.
40 A. Navulla, L. Huynh, Z. Wei, A. S. Filatov and E. V. Dikarev, *J. Am. Chem. Soc.*, 2012, **134**, 5762–5765.
41 Z. Wei, H. Han, A. S. Filatov and E. V. Dikarev, *Chem. Sci.*, 2014, **5**, 813–818.
42 M. C. Barry, Z. Wei, T. He, A. S. Filatov and E. V. Dikarev, *J. Am. Chem. Soc.*, 2016, **138**, 8883–8887.
43 Z. Wei, A. S. Filatov and E. V. Dikarev, *J. Am. Chem. Soc.*, 2013, **135**, 12216–12219.
44 T. J. Boyle, M. L. Neville, C. A. Apblett, S. M. Hoppe and M. Gembicky, *Polyhedron*, 2013, **65**, 89–97.
45 M. Tiitta and L. Niinistou, *Chem. Vap. Deposition*, 1997, **3**, 167–182.
46 V. G. Kessler, *Chem. Commun.*, 2003, 1213–1222.
47 H. Han, Z. Wei, M. C. Barry, A. S. Filatov and E. V. Dikarev, *Dalton Trans.*, 2017, **46**, 5644–5649.
48 M. Nespolo, G. Ferraris and H. Takeda, *Acta Crystallogr., Sect. A: Found. Adv.*, 2000, **56**, 132–148.
49 C. M. Lieberman, M. C. Barry, Z. Wei, A. Y. Rogachev, X. Wang, J.-L. Liu, R. Clérac, Y.-S. Chen, A. S. Filatov and E. V. Dikarev, *Inorg. Chem.*, 2017, **56**, 9574–9584.
50 V. Subramanian, K. Karki and B. Rambabu, *Solid State Ionics*, 2004, **175**, 315–318.
51 Y.-K. Sun, I.-H. Oh and K. Y. Kim, *J. Mater. Chem.*, 1997, **7**, 1481–1485.
52 J. Akimoto, Y. Gotoh and Y. Oosawa, *J. Solid State Chem.*, 1998, **141**, 298–302.